ICES Report 04-02

Added-mass effect in the design of partitioned algorithms for fluid-structure problems

Paola Causin[1], Jean-Frédéric Gerbeau[1], Fabio Nobile[2]

[1] INRIA Rocquencourt, Domaine de Voluceau, Rocquencourt B.P. 105
78153 Le Chesnay Cedex, France

[2] ICES, The University of Texas at Austin, Texas 78712, U.S.A.

Abstract

The aim of this work is to provide a mathematical contribution to explain the numerical instabilities encountered under certain combinations of physical parameters in the simulation of fluid-structure interaction (FSI) when using loosely coupled time advancing schemes. It is also shown how the same combinations of parameters lead, in the case of strongly coupled schemes, to problems that demand a greater computational effort to be solved, requiring for example a high number of subiterations. The application that we have in mind is FSI simulation for blood flow in large human arteries, but the discussion applies as well to several FSI problems in which an incompressible fluid interacts with a thin elastic structure. To carry out the mathematical analysis, we consider a simplified model representing the interaction between a potential fluid and a linear elastic thin tube. Despite its simplicity, this model reproduces propagation phenomena and takes into account the added-mass effect of the fluid on the structure, which is known to be source of numerical difficulties. This allows to draw conclusions that apply to more realistic problems, as well.

1 Introduction

In this work we focus our attention on the numerical simulation of an incompressible fluid interacting with a thin elastic structure. The target application is the simulation of blood flow in large arteries, although the analysis presented here applies to a much wider class of fluid-structure interaction (FSI) problems.

Among the most used numerical techniques in this context are the so-called "partitioned" time marching algorithms, which are based on subsequent solutions of the fluid and structure subproblems and allow one to reuse existing computational codes (see e.g. [21, 20, 17, 5, 4, 11, 12])

Although loosely coupled (explicit) algorithms are successfully used in aeroelasticity (see [5] and the references therein), it is common experience in other applications [19, 10, 16] that they feature instabilities under certain choices of the physical parameters, typically when the densities of the fluid and the structure are comparable or when the domain has a slender shape, irrespectively of the choice of the time step. Conversely, strongly coupled (implicit) algorithms feature convergence problems under the same conditions. These issues are still not well understood and, in particular, very few mathematical explanations and mathematically formulated stability or convergence conditions are available, so far, also because of the high complexity and nonlinearity of FSI problems.

The goal of this work is to provide a tool for the study of the stability and/or the convergence analysis of partitioned coupled algorithms, which is based on a "toy FSI model" that represents the interaction between a potential fluid and a linear elastic thin tube. We do not claim that this model is relevant to properly describe complex situations, like fluid-structure interaction in arteries since, for example, it does not include nonlinearities and dissipation phenomena. Nevertheless, it retains important physical features common to more complex models: in particular, it reproduces propagation phenomena and takes into account the added-mass effect of the fluid on the structure, which is known to induce numerical difficulties [10]. This model problem is simple enough to perform mathematical and numerical studies but, at the same time, complex enough to mimic more realistic situations, at least in the case of incompressible fluids. As it will be shown in Sections 5 and 6, starting from this simple FSI model, we are able to derive stability and convergence conditions that are in excellent agreement with the numerical observations collected in much more complex situations. Moreover, this toy FSI model, and the type of analysis proposed in this paper, may be helpful also in devising new and, possibly, more efficient coupled algorithms.

The work is organized as follows. In Sect. 2 we give some details on empirical observations and results concerning the stability of partitioned algorithms. In Sect. 3 we present the simplified fluid-structure model on which we are going to carry out our analysis. In Sect. 4 we introduce the functional setting and we present the FSI problem as a structure equation modified by the introduction of an added-mass operator that represents the effect of the fluid on the structure itself. In Sect. 5 and 6 we consider different explicit and implicit schemes to advance in time the interface FSI problem and we propose mathematical criteria to individuate range of values of the physical parameters leading to numerical instabilities. In Sect. 7 we briefly address the space discretization of the FSI problem and we present numerical results that validate the mathematical analysis of the preceding section. Finally, in Sect. 8 we use scaling arguments to reproduce and extend to a wider spectrum of situations, even if in a more qualitative way, the results of Sect. 5 and 6.

2 Motivations

In order to motivate the main results of this article, we recall some empirical observations made on a basic FSI test case proposed in previous studies (see [6, 7, 16]). The goal of this test case is to simulate, in a very idealized framework, the mechanical interaction between blood and arterial wall. The geometry at rest is a cylinder. The fluid is described by the incompressible Navier-Stokes equations in Arbitrary Lagrangian Eulerian formulation. The structure is described either by a 1D generalized string model (for 2D simulations) or by a nonlinear shell model in large displacements regime (for 3D simulations). An overpressure is applied at the inlet of the fluid for a short duration of time. Although the fluid is incompressible, there is a finite velocity propagation of the overpressure due the fluid-structure coupling. Fig 1 shows the propagation phenomenon in 2D. The 3D case gives analogous results (see [7]). All the details regarding this test case can be found in the above cited references.

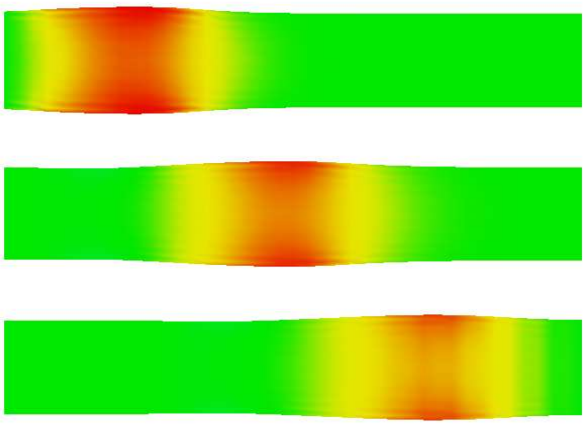

Figure 1: Propagation of a pressure wave in a portion of artery (2D), t=6, 10 and 14 ms.

We first tried explicit (or "loosely") coupled methods, *i.e.* roughly speaking, algorithms which do not ensure exact balance of energy, but which only require one fluid and one structure resolution per time step.

It was observed that these algorithms exhibit numerical instabilities

(R1) for a given geometry, as soon as the density of the structure is lower than a certain threshold;

(R2) for a given structure density, as soon as the length of the domain is greater than a certain threshold.

We then tried "strongly" coupled methods, *i.e.* we ensure at each time step an exact balance of energy by sub-iterating several times between the fluid and the structure. When the subiterations consist of a relaxed fixed-point method, it was observed that an increasing amount of relaxation is needed when

(R3) the density of the structure decreases;

(R4) the length of the domain increases.

All the details concerning these observations (values of parameters, algorithms, experiments, *etc.*) can be found in [16, Chap.4].

The fact that the numerical stability depends on the structure density has a clear physical interpretation. This is not the same for the dependence on the geometry, which is quite amazing: since the main physical phenomenon is a wave propagation with a *finite* velocity, it is surprising that the length of the domain modifies the stability of the algorithm (independently of the space and time steps).

It is quite difficult to explain these observations on the original fully nonlinear equations. That is why we propose in the next section a simplified model which exhibits an analogous behavior and which is simple enough to be analyzed in detail.

Moreover, the simplified model is also a good candidate for testing new approaches. As an example, we consider in Sect. 6.2 a possible alternative to the Dirichlet/Neumann iterations classically used in fluid-structure simulations.

3 A simplified fluid-structure problem

We consider a rectangular domain $\Omega_F \subset \mathbb{R}^2$ whose boundary is split into Γ_F^1, Γ_F^2, Γ_F^3 and Σ (see Fig. 2). The part Σ corresponds to the fluid-structure interface. In this simplified model, the domain Ω_S occupied by the structure is such that $\overline{\Omega}_S = \Sigma$. We set $\Gamma_F = \Gamma_F^1 \cup \Gamma_F^2$. We denote by $\mathbf{n}$ the unit outward normal vector on $\partial\Omega_F$

3.1 The structural problem

In the domain Ω_S we use a structural model derived from the theory of linear elasticity for a cylindrical tube with small thickness, under the assumption of membrane deformations. The reference configuration is a cylindrical surface of base circle radius R that is supposed to move only radially, the longitudinal and angular displacements being neglected. Intersecting the cylindrical tube with the plane $\theta = \bar{\theta}$ we obtain the following generalized string model: find the displacement $\eta = \eta(t, x)$ such that

$$\begin{cases} \varrho_s h_s \dfrac{\partial^2 \eta}{\partial t^2} + a\eta - b\dfrac{\partial^2 \eta}{\partial x^2} = f & \text{in } (0,T)\times\Omega_S, \\ \eta = 0 \quad \text{on } (0,T)\times\partial\Omega_s, \end{cases} \tag{1}$$

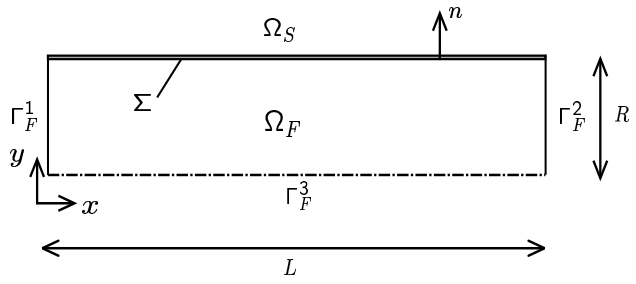

Figure 2: Schematic representation of the computational domain (the dashed line represents the symmetry axis).

where h_s is the thickness of the structure and ϱ_s its mass per unit volume, $a = Eh_s/R^2(1-\nu^2)$, E being the Young modulus and ν the Poisson coefficient, $b = \kappa_T G h_s$, G being the shear stress modulus, κ_T the Timoshenko shear correction factor, and f the external forcing term coming from the fluid (whose expression will be made precise in the following). Equation (1) must be supplied with initial conditions

$$\eta(0,x) = \eta_0(x), \qquad \frac{\partial \eta}{\partial t}(0,x) = \dot{\eta}_0(x) \quad \text{in } \Omega_S, \tag{2}$$

and boundary conditions $\eta(t,0) = \eta(t,L) = 0, \forall t \in (0,T)$.

3.2 The fluid problem

For the fluid, we use a linear incompressible inviscid model. Moreover, the deformation η of the structure is assumed to be very small, so that the fluid domain Ω_F can be considered fixed. Thus, the fluid problem reads:

find the fluid velocity $\mathbf{u} = \mathbf{u}(t,x,y)$ and pressure $p = p(t,x,y)$ such that

$$\begin{cases} \varrho_f \dfrac{\partial \mathbf{u}}{\partial t} + \nabla p = 0 & \text{in } (0,T)\times\Omega_F, \\ \operatorname{div} \mathbf{u} = 0 & \text{in } (0,T)\times\Omega_F, \\ p = \overline{p}(t) & \text{on } \Gamma_F^1 \cup \Gamma_F^2, \\ \mathbf{u}\cdot\mathbf{n} = 0 & \text{on } \Gamma_F^3, \\ \mathbf{u}\cdot\mathbf{n} = w & \text{on } \Sigma, \end{cases} \tag{3}$$

where ϱ_f is the fluid mass per unit volume and where $\overline{p}$ and w are given functions (we refer to Fig. 2 for the notations). System (3) may be conveniently

reformulated as follows:

$$\begin{cases} -\triangle p &= 0 & \text{in } \Omega_F, \\ p &= \overline{p}(t) & \text{on } \Gamma_F^1 \cup \Gamma_F^2, \\ \dfrac{\partial p}{\partial n} &= 0 & \text{on } \Gamma_F^3, \\ \dfrac{\partial p}{\partial n} &= -\varrho_f \dfrac{\partial w}{\partial t} & \text{on } \Sigma. \end{cases} \tag{4}$$

3.3 Fluid-structure interaction

The fluid and structure systems are coupled by the following conditions

$$\begin{cases} \mathbf{u} \cdot \mathbf{n} = w = \dfrac{\partial \eta}{\partial t} & \text{on } \Sigma, \\ f = p & \text{on } \Sigma. \end{cases} \tag{5}$$

The first equation is the kinematic compatibility condition, where we have used the geometrical assumption that Ω_F does not change with time. The second condition in (5) transfers the pressure load from the fluid to the structure as a volume force for this latter, this being in the simplified model the only contribution coming from the fluid.

Using $(5)_1$, condition $(4)_4$ may be conveniently written as

$$\frac{\partial p}{\partial n} = -\varrho_f \frac{\partial^2 \eta}{\partial t^2} \qquad \text{on } \Sigma. \tag{6}$$

4 Mathematical preliminaries

4.1 Functional setting

We introduce the functional spaces

$$V = H_0^1(\Omega_S),$$

$$Q = \{q \in H^1(\Omega_F), q|_{\Gamma_F^1 \cup \Gamma_F^2} = 0\}.$$

We denote by $(\cdot, \cdot)$ the $L^2(\Omega_F)$ or $L^2(\Omega_S)$ inner products and we define the bilinear forms:

$$a_F(p, q) = \int_{\Omega_F} \nabla p \cdot \nabla q \, dx \, dy \qquad \forall p, q \in H^1(\Omega_F),$$

$$a_S(\eta, \xi) = \int_{\Omega_S} a \, \eta \, \xi \, dx + \int_{\Omega_S} b \frac{\partial \eta}{\partial x} \frac{\partial \xi}{\partial x} \, dx \qquad \forall \eta, \xi \in H^1(\Omega_S).$$

In all this Section, the Hilbert space V will be endowed with the scalar product defined by $a_S(\cdot, \cdot)$. We make the following regularity assumptions on the boundary data for the fluid

$$\overline{p} \in \mathcal{C}(0, \infty; H^{1/2}(\Gamma_F)), \tag{7}$$

and on the initial data for the structure

$$\eta_0 \in V, \dot{\eta}_0 \in V. \tag{8}$$

In the following, we will make use of the notation q_Σ to indicate the restriction of the function $q : \Omega_F \to \mathbb{R}$ to the interface Σ.

A variational formulation of the fluid-structure problem introduced in the previous section is:
find $(p, \eta) \in \mathcal{C}(0, \infty; H^1(\Omega_F)) \times \mathcal{C}(0, \infty; V)$ such that (2) is satisfied, $p(t)|_{\Gamma_F^1 \cup \Gamma_F^2} = \overline{p}(t)$, $\forall t \in (0, \infty)$ and for all $(q, \xi) \in Q \times V$:

$$\left\{ \begin{array}{rcl} a_F(p, q) & = & -\varrho_f \displaystyle\int_\Sigma \frac{\partial^2 \eta}{\partial t^2} q \\ \left(\varrho_s h_s \dfrac{\partial^2 \eta}{\partial t^2}, \xi \right) + a_S(\eta, \xi) & = & (p|_\Sigma, \xi). \end{array} \right. \tag{9}$$

In order to write problem (9) in a more compact form, some additional notation is needed. We introduce the following operators: for $\eta, \xi \in V$, we define

$$< \mathcal{L}\eta, \xi >= a_S(\eta, \xi) \tag{10}$$

and for $\ell \in L^2(\Omega_S)$, we denote by $T\ell$ the element of V such that

$$< \mathcal{L}(T\ell), \xi >= (\ell, \xi). \tag{11}$$

Using the above definitions, the structure problem reads:
find η such that

$$\varrho_s h_s \frac{\partial^2 \eta}{\partial t^2} + \mathcal{L}\eta = p_\Sigma. \tag{12}$$

Next, for any $w \in H^{-1/2}(\Sigma)$, we denote by $\mathcal{R}w$ the element of Q solution of the following problem

$$\left\{ \begin{array}{rcll} -\Delta \mathcal{R}w & = & 0 & \text{in } \Omega_F, \\ \mathcal{R}w & = & 0 & \text{on } \Gamma_F^1 \cup \Gamma_F^2, \\ \dfrac{\partial \mathcal{R}w}{\partial n} & = & 0 & \text{on } \Gamma_F^3, \\ \dfrac{\partial \mathcal{R}w}{\partial n} & = & w & \text{on } \Sigma. \end{array} \right. \tag{13}$$

We define the operator $\mathcal{M}_\mathcal{A} : H^{-1/2}(\Sigma) \to H^{1/2}(\Sigma)$ by

$$\mathcal{M}_\mathcal{A} w = \mathcal{R}w|_\Sigma. \tag{14}$$

Note that, for $w, v \in L^2(\Sigma)$,

$$< \mathcal{M}_\mathcal{A} w, v >= a_F(\mathcal{R}w, \mathcal{R}v).$$

We gather in the following proposition some standard results ([3, 8]):

Proposition 1

1. *The operator $T : L^2(\Omega_S) \to V$ is compact self-adjoint and positive on V;*
2. *the operator $\mathcal{M}_{\mathcal{A}} : H^{-1/2}(\Sigma) \to H^{1/2}(\Sigma)$ is continuous;*
3. *the operator $\mathcal{M}_{\mathcal{A}}$ is compact, self-adjoint and positive on $L^2(\Sigma)$.*

Let us now introduce an arbitrary continuous extension operator $E_F : H^{1/2}(\Gamma_F) \to H^1(\Omega_F)$. By definition, for $q \in H^{1/2}(\Gamma_F)$, $E_F q|_{\Gamma_F} = q$ and $\|E_F q\|_{H^1(\Omega_F)} \leq C\|q\|_{H^{1/2}(\Gamma_F)}$.

We define $p^* \in \mathcal{C}(0,\infty; H^1(\Omega_F))$ as the solution to

$$\left\{\begin{array}{rcll} -\Delta p^* & = & \triangle E_F\overline{p} & \text{in } \Omega_F, \\ p^* & = & 0 & \text{on } \Gamma_F^1 \cup \Gamma_F^2, \\ \dfrac{\partial p^*}{\partial n} & = & -\dfrac{\partial E_F\overline{p}}{\partial n} & \text{on } \Gamma_F^3, \\ \dfrac{\partial p^*}{\partial n} & = & -\dfrac{\partial E_F\overline{p}}{\partial n} & \text{on } \Sigma. \end{array}\right. \tag{15}$$

Using equations (13) and (15), the solution to (4) is given by

$$p = p^* + E_F\overline{p} - \varrho_f \mathcal{R}\frac{\partial^2 \eta}{\partial t^2}. \tag{16}$$

Then, defining

$$p_{ext} = p^*|_\Sigma + E_F\overline{p}|_\Sigma, \tag{17}$$

and using (14), we have

$$p_\Sigma = p_{ext} - \varrho_f \mathcal{M}_{\mathcal{A}}\frac{\partial^2 \eta}{\partial t^2}. \tag{18}$$

Let $\mathcal{I}$ denote the identity operator. Plugging (18) into (12), we see that (9) can be written in the following form:
find η such that

$$(\varrho_s h_s \mathcal{I} + \varrho_f \mathcal{M}_{\mathcal{A}})\frac{\partial^2 \eta}{\partial t^2} + \mathcal{L}\eta = p_{ext}, \tag{19}$$

the pressure in the fluid being given by (16). The following result holds.

Proposition 2 *Under assumptions (7) and (8) on the data, there exists a unique solution $\eta \in \mathcal{C}([0,\infty); V)$ to equation (19) satisfying the initial conditions (2). Moreover, $\dfrac{\partial \eta}{\partial t} \in \mathcal{C}([0,\infty); L^2(\Sigma))$.*

Sketch of the proof.

This proposition is just a variant of a result proved in [8]. The main ingredient is to notice that the operator:

$$\mathcal{A} = T(\varrho_s h_s \mathcal{I} + \varrho_f \mathcal{M}_{\mathcal{A}})$$

is compact, self-adjoint and positive on V (endowed with the scalar product $a_S(\cdot,\cdot)$, which straightforwardly comes from Proposition 1 (recall (11)). Consequently, there exists a complete orthogonal sequence in V made by the eigenfunctions of $\mathcal{A}$. The existence of the solution to (19) can then be obtained in a standard way, by using this basis in the Faedo-Galerkin method for example.□

Remark 1 *Equation (19) looks like the structure equation (12) except for the extra operator $\varrho_f \mathcal{M}_\mathcal{A}$ in front of the second order time derivative. This operator represents the interaction of the fluid on the structure and acts as an extra mass (hence the name of "added-mass" effect). In particular, the presence of the fluid changes the natural vibration frequencies of the structure. We refer the interested reader to [9, 13, 14].*

4.2 Spectrum of the added-mass operator

In order to carry out the subsequent mathematical analysis, it is convenient to dispose of an estimate of the maximum eigenvalue of $\mathcal{M}_\mathcal{A}$, that we will denote by μ_{max}. Note that the inverse of μ_{max} is the smallest eigenvalue of the standard Steklov-Poincaré operator [18]. Note also that μ_{max} is a purely geometric quantity.

When dealing with a generic geometry, a closed expression for μ_{max} cannot be found. The procedure that can be followed then is the analysis proposed in [2] (see also [1]), adapted to a single subdomain problem. The indication provided by such an estimate is that the overall effect of an increase of the domain diameter is an increase of the largest eigenvalue of $\mathcal{M}_\mathcal{A}$. Nevertheless, it may be difficult to sharply separate the effects of the increase of diameter from the effects of the increase of the aspect ratio.

In the case of the simple geometry of Fig. 2, μ_{max} can be computed analytically. To do this, we consider the following problem:
find $u = u(x,y)$ such that

$$\left\{\begin{array}{rcll} -\triangle u & = & 0 & \text{in } \Omega_F, \\ u & = & 0 & \text{on } \Gamma_F^1 \cup \Gamma_F^2, \\ \dfrac{\partial u}{\partial y} & = & 0 & \text{on } \Gamma_F^3, \\ \dfrac{\partial u}{\partial y} & = & g & \text{on } \Sigma, \end{array}\right. \tag{20}$$

where $g = g(x)$ is a prescribed function such that $g(0) = g(L) = 0$. Expressing g as the superposition $g = \displaystyle\sum_{k\geq 1} g_k \sin\left(\frac{k\pi}{L}x\right)$, allows us to obtain the solution to (20)

$$u(x,y) = \sum_{k\geq 1} g_k \frac{L}{k\pi} \sin\left(\frac{k\pi x}{L}\right) \frac{\mathrm{ch}\left(\dfrac{k\pi y}{L}\right)}{\mathrm{sh}\left(\dfrac{k\pi R}{L}\right)}.$$

Recalling definition (14), we can write

$$\mathcal{M}_{\mathcal{A}} g = u|_{y=R} = \sum_{k\geq 1} g_k \frac{L}{k\pi \mathrm{th}\left(\frac{k\pi R}{L}\right)} \sin\left(\frac{k\pi x}{L}\right).$$

Finding the eigenvalue $\mu_n, n = 1, 2, \ldots,$ of $\mathcal{M}_{\mathcal{A}}$ associated to the eigenvector $g = g_n \sin\left(\frac{n\pi}{L}x\right)$ amounts to solving the eigenvalue problem

$$\mathcal{M}_{\mathcal{A}} g = \mu_n g,$$

which yields

$$\mu_n = \frac{L}{n\pi \mathrm{th}\left(\frac{n\pi R}{L}\right)}.$$

The largest eigenvalue μ_{max}, corresponding to $n = 1$, is thus

$$\mu_{max} = \frac{L}{\pi \mathrm{th}\left(\frac{\pi R}{L}\right)}. \tag{21}$$

Figure 3 shows the value of μ_{max} for different values of L and R.

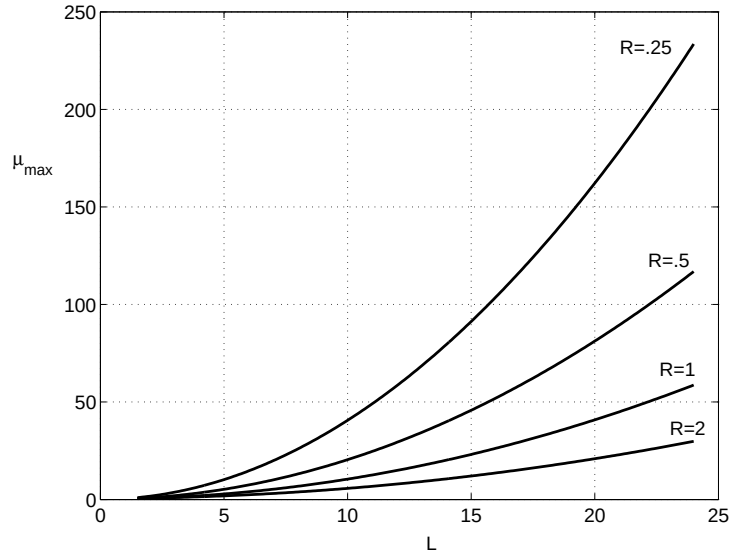

Figure 3: Largest eigenvalue of $\mathcal{M}_{\mathcal{A}}$ given by (21) as a function of the domain length L and height R.

5 Stability of explicit time-marching schemes

We present in this section a stability analysis of an explicit time-marching scheme for the temporal discretization of the FSI problem presented in Sect. 3. The space discretization will be addressed in the next section. Moreover, for the sake of simplicity and under the scaling considerations presented in Sect. 8 for the problem at hand, we assume that the coefficient b in (1) is zero. The differential structural operator defined in (10) therefore reduces to $\mathcal{L}\eta = a\eta$. The results obtained in the next sections generalize easily to the case $b \neq 0$.

By explicit time marching schemes we mean time discretization algorithms of the coupled FSI problem (1), (2), (3), (5) that allow to solve only once (or just a few times) the fluid and the structure equations within each time step. They can be typically obtained by combining an explicit algorithm for one of the subsystems (either fluid or structure) with an implicit one for the other subsystem.

Our goal is to show that those kind of algorithms might be *unconditionally unstable* in certain cases, depending on the relative mass density of the structure and the fluid and on some geometric properties of the domain.

As a prototype of an explicit algorithm, we consider the one obtained by employing a Leap-Frog scheme for the structure and an Implicit Euler scheme for the fluid (LF-IE scheme).

Denoting by δt the time step, the time-discrete system that we consider is the following:

$$\left\{\begin{array}{rcll} \varrho_f \dfrac{\mathbf{u}^n - \mathbf{u}^{n-1}}{\delta t} + \nabla p^n &=& 0 & \text{in } \Omega_F, \\ \operatorname{div} \mathbf{u}^n &=& 0 & \text{in } \Omega_F, \\ p^n &=& \overline{p}(t^n) & \text{on } \Gamma_F^1 \cup \Gamma_F^2, \\ \mathbf{u}^n \cdot \mathbf{n} &=& 0 & \text{on } \Gamma_F^3, \end{array}\right. \tag{22}$$

and

$$\mathbf{u}^n \cdot \mathbf{n} = \frac{\eta^n - \eta^{n-1}}{\delta t} \qquad \text{on } \Sigma, \tag{23}$$

$$\varrho_s h_s \frac{\eta^{n+1} - 2\eta^n + \eta^{n-1}}{\delta t^2} + a\eta^n = p^n \qquad \text{in } \Omega_S. \tag{24}$$

Observe that, given the wall displacement η^n at time t^n, the fluid equation (22) with boundary condition (23) allows to compute the fluid velocity $\mathbf{u}^n$ and pressure p^n. With this latter, we can now solve the structure equation (24) and get the new wall displacement η^{n+1} at time t^{n+1}. Hence, this coupling algorithm is explicit.

We now analyze its stability. We proceed as in Sect. 4.1 and we reduce the

coupled problem to a single structure equation with added-mass. We have:

$$\begin{cases} \Delta p^n = 0 & \text{in } \Omega \\ \dfrac{\partial p^n}{\partial \mathbf{n}} = -\varrho_f \dfrac{(\mathbf{u}^n - \mathbf{u}^{n-1}) \cdot \mathbf{n}}{\delta t} = -\varrho_f \dfrac{\eta^n - 2\eta^{n-1} + \eta^{n-2}}{\delta t^2} & \text{on } \Sigma \\ \dfrac{\partial p^n}{\partial \mathbf{n}} = 0 & \text{on } \Gamma_F^3 \\ p^n = \overline{p}(t^n) & \text{on } \Gamma_F. \end{cases}$$

Hence, with the notation introduced in (17), we have

$$p^n\big|_\Sigma = p^n_{ext} - \varrho_f \mathcal{M}_\mathcal{A} \frac{\eta^n - 2\eta^{n-1} + \eta^{n-2}}{\delta t^2},$$

and

$$\varrho_s h_s \frac{\eta^{n+1} - 2\eta^n + \eta^{n-1}}{\delta t^2} + \varrho_f \mathcal{M}_\mathcal{A} \frac{\eta^n - 2\eta^{n-1} + \eta^{n-2}}{\delta t^2} + a\eta^n = p^n_{ext} \qquad \text{on } \Omega_S. \tag{25}$$

The following result holds

Proposition 3 *Let μ_{max} be the largest eigenvalue of the operator $\mathcal{M}_\mathcal{A}$. Then, the scheme (25), and hence the coupled explicit algorithm (22)-(24), is unconditionally unstable if*

$$\boxed{\frac{\varrho_s h_s}{\varrho_f \mu_{max}} < 1} \tag{26}$$

Proof. From the compactness of the operator $\mathcal{M}_\mathcal{A}$ (see Proposition 1), we know that there exists an orthonormal Hilbert basis of $L^2(\Sigma)$, made of eigenvectors $\{z_i\}$ of $\mathcal{M}_\mathcal{A}$. We thus expand the solution η and the right-hand side p_{ext} on this basis: $\eta^n = \sum_i \eta_i^n \, z_i$ and $p^n_{ext} = \sum_i (p^n_{ext})_i \, z_i$. Each Fourier coefficient η_i of the solution satisfies

$$\varrho_s h_s \frac{\eta_i^{n+1} - 2\eta_i^n + \eta_i^{n-1}}{\delta t^2} + \varrho_f \mu_i \frac{\eta_i^n - 2\eta_i^{n-1} + \eta_i^{n-2}}{\delta t^2} + a\eta_i^n = (p^n_{ext})_i \,,$$

μ_i being the eigenvalue associated to z_i.

By direct calculation, the characteristic polynomial $\chi(s) \in \mathbb{P}^3$ of the previous difference equation satisfies:

$$\chi(-\infty) = -\infty \qquad \text{and} \qquad \chi(-1) = a + \frac{4}{\delta t^2}(\varrho_f \mu_i - \varrho_s h_s). \tag{27}$$

It follows that, if $\varrho_f \mu_i > \varrho_s h_s$ for some i, then $\chi(-1) > 0$ and there exists a root s^* of $\chi(s)$ such that $s^* < -1$. In particular, we can conclude that, if $\varrho_f \mu_{max} > \varrho_s h_s$, the difference equation (25) is unstable irrespectively of the time step. □

Remark 2 *Observe that the "instability" condition (26) confirms empirical observations (R1) and (R2) of Sect. 2. Indeed, this condition is more and more restrictive as $\varrho_s h_s/\varrho_f$ decreases and as μ_{max} increases, the connection of this latter with the geometry being shown in* (21)*. Namely, the more Ω_F becomes a slender geometry (that is when, for a fixed radius R, L increases or when, for a fixed length L, R decreases), the larger μ_{max} becomes (see also Fig. 3).*

Remark 3 *In view of (27), it appears that even when $\varrho_s h_s/\varrho_f \mu_{max} > 1$ (that is when, for example, the structure is much denser than the fluid), instabilities may occur if the positive parameter a is large enough (*e.g. *when the structure is characterized by a large Young modulus). Nevertheless, in such a case, the scheme can be stabilized by suitably decreasing the time step. This situation will be addressed more in detail in Sect. 8.*

6 Implicit time-marching schemes

Proposition 3 suggests that explicit coupling algorithms might not work for fluid-structure interaction problems in certain conditions. An obvious remedy consists in switching to implicit couplings. As a prototype of implicit coupling algorithms we choose here the one obtained by combining the Implicit Euler scheme for the fluid with the first order backward difference scheme for the structure (IE-BDF scheme). The time-discrete problem reads:

$$\left\{\begin{array}{rcll} \varrho_f \dfrac{\mathbf{u}^{n+1}-\mathbf{u}^n}{\delta t} + \nabla p^{n+1} &=& 0 & \text{in } \Omega_F, \\ \operatorname{div} \mathbf{u}^{n+1} &=& 0 & \text{in } \Omega_F, \\ p^{n+1} &=& \overline{p}(t^{n+1}) & \text{on } \Gamma_F^1 \cup \Gamma_F^2, \\ \mathbf{u}^{n+1}\cdot\mathbf{n} &=& 0 & \text{on } \Gamma_F^3, \end{array}\right. \tag{28}$$

and

$$\mathbf{u}^{n+1}\cdot\mathbf{n} = \frac{\eta^{n+1}-\eta^n}{\delta t} \qquad \text{on } \Sigma, \tag{29}$$

$$\varrho_s h_s \frac{\eta^{n+1}-2\eta^n+\eta^{n-1}}{\delta t^2} + a\eta^{n+1} = p^{n+1} \qquad \text{on } \Omega_S. \tag{30}$$

This problem corresponds to the following discrete added-mass problem for the structure

$$(\varrho_s h_s + \varrho_f \mathcal{M}_{\mathcal{A}}) \frac{\eta^{n+1}-2\eta^n+\eta^{n-1}}{\delta t^2} + a\eta^{n+1} = p_{ext}^{n+1} \qquad \text{in } \Omega_S. \tag{31}$$

It is straightforward to show that problem (31), and hence the coupled problem (28)-(30), is stable for any choice of the time step δt.

In this simple example, at each time step, the coupled problem (28)-(30) turns into a linear system in the unknowns $(\mathbf{u}^{n+1}, p^{n+1}, \eta^{n+1})$ (after spatial discretization) and can be assembled and solved quite easily. Yet, in more realistic

(and complex) situations, the problem might be non linear (non-linearities in the fluid and/or structure equations and possibly large displacements of the structure). Then, in order to solve (28)-(30) at each time step, it is often convenient to consider iterative methods; this approach allow to decouple the fluid from the structure step and, ultimately, to use already available computer codes.

In the next two subsections we will analyze two possible iterative methods that we will call *Dirichlet/Neumann* and *Neumann/Dirichlet*, borrowing the terminology from corresponding Domain Decomposition algorithms [18]. By Dirichlet/Neumann (D-N) method we mean that at each iteration we solve the fluid equations with respect to primitive variables $(\mathbf{u}, p)$ subject to Dirichlet boundary conditions at the interface (imposed displacements or velocities) and the structure equations subject to Neumann boundary conditions (imposed loads). The Neumann/Dirichlet (N-D) method is carried out with a procedure dual to the one above described.

6.1 Dirichlet/Neumann subiterations

At each time step, we use the following algorithm to solve (28)-(30):

given an initial guess η_0^{n+1}*, we solve for each* $k = 1, 2, \ldots$

1. Fluid step: find $(\mathbf{u}_k, p_k)$ s.t.

$$\begin{cases} \varrho_f \dfrac{\mathbf{u}_k - \mathbf{u}^n}{\delta t} + \nabla p_k = 0 & \text{in } \Omega_F, \\ \operatorname{div} \mathbf{u}_k = 0 & \text{in } \Omega_F, \\ p_k = \overline{p}(t^{n+1}) & \text{on } \Gamma_F^1 \cup \Gamma_F^2, \\ \mathbf{u}_k \cdot \mathbf{n} = 0 & \text{on } \Gamma_F^3, \\ \mathbf{u}_k \cdot \mathbf{n} = \dfrac{\eta_{k-1} - \eta^n}{\delta t} & \text{on } \Sigma. \end{cases}$$

2. Structure step: find $\tilde{\eta}_k$ s.t.

$$\varrho_s h_s \frac{\tilde{\eta}_k - 2\eta^n + \eta^{n-1}}{\delta t^2} + a\tilde{\eta}_k = p_k \qquad \text{in } \Omega_S.$$

3. Relaxation step:

$$\eta_k = \omega\tilde{\eta}_k + (1-\omega)\eta_{k-1}.$$

4. Convergence test:

   - if $||\eta_k - \eta_{k-1}|| < tol$ then set $\eta^{n+1} = \eta_k$, $\mathbf{u}^{n+1} = \mathbf{u}_k$ and $p^{n+1} = p_k$
   - else set $k = k+1$ and go to step 1.

We can eliminate the unknowns $\mathbf{u}_k$ and p_k, using the same technique employed before. We obtain in this case:

$$p_{\Sigma,k} = -\varrho_f \mathcal{M}_{\mathcal{A}} \left(\frac{\eta_{k-1} - 2\eta^n + \eta^{n-1}}{\delta t^2} \right) + p_{ext}^{n+1}.$$

Keeping in mind that $\tilde{\eta}_k = \dfrac{\eta_k}{\omega} - \dfrac{1-\omega}{\omega}\eta_{k-1}$, the previous algorithm corresponds to the following iterative method to solve the added-mass problem (31):

$$\frac{\varrho_s h_s}{\delta t^2}\left(\frac{\eta_k}{\omega} - 2\eta^n + \eta^{n-1}\right) + a\frac{\eta_k}{\omega} = \frac{1-\omega}{\omega}\left(\frac{\varrho_s h_s}{\delta t^2} + a\right)\eta_{k-1} \\ - \varrho_f \mathcal{M}_{\mathcal{A}}\left(\frac{\eta_{k-1} - 2\eta^n + \eta^{n-1}}{\delta t^2}\right) + p_{ext}^{n+1}, \qquad k = 1, 2, \ldots$$

or, equivalently, the fixed-point iteration

$$\frac{1}{\omega}\left(\frac{\varrho_s h_s}{\delta t^2} + a\right)\eta_k = \left[\frac{1-\omega}{\omega}\left(\frac{\varrho_s h_s}{\delta t^2} + a\right) - \frac{\varrho_f \mathcal{M}_{\mathcal{A}}}{\delta t^2}\right]\eta_{k-1} + g(\eta^n, \eta^{n+1}, p_{ext}^{n+1}). \tag{32}$$

Concerning the convergence of the fixed point iteration (32), we state the following

Proposition 4 *The D-N iterative method converges to the solution to (28)-(30) if and only if*

$$\boxed{0 < \omega < \frac{2(\varrho_s h_s + a\delta t^2)}{\varrho_s h_s + \varrho_f \mu_{max} + a\delta t^2}} \tag{33}$$

Proof. The solution η^{n+1} to (28)-(30) is the fixed point of the iterative method (32) and a necessary and sufficient condition for the convergence of this latter is

$$\left|\frac{(1-\omega)(\varrho_s h_s + a\delta t^2) - \omega\varrho_f \mu_i}{\varrho_s h_s + a\delta t^2}\right| < 1.$$

A straightforward calculation leads to (33). □

Remark 4 *This result confirms the empirical observations (R3) and (R4) of Sect. 2 (see also Remark 2).*

Remark 5 *In the limit $\delta t \to 0$, condition (33) reads*

$$0 < \omega < \frac{2}{1 + \varrho_f \mu_{max}/(\varrho_s h_s)}.$$

Observe that, in this case, whenever the explicit algorithm diverges ($\varrho_f \mu_{max} > \varrho_s h_s$), the D-N iterative method needs a relaxation parameter strictly smaller than 1 to converge.

6.2 Neumann/Dirichlet subiterations

The aim of this Section is to investigate a possible alternative to the standard Dirichlet/Neumann iterations. We consider the following scheme:

given an initial guess η_0^{n+1}, we solve for each $k = 1, 2, \ldots$

1. Structure step: compute the load ϕ_k s.t.

$$\phi_k = \varrho_s h_s \frac{\eta_{k-1} - 2\eta^n + \eta^{n-1}}{\delta t^2} + a\eta_{k-1} - p_{ext}^{n+1} \qquad \text{in } \Omega_S.$$

2. Fluid step: find $(\mathbf{u}_k, p_k)$ s.t.

$$\begin{cases} \varrho_f \dfrac{\mathbf{u}_k - \mathbf{u}^n}{\delta t} + \nabla p_k &= 0 & \text{in } \Omega_F, \\ \operatorname{div} \mathbf{u}_k &= 0 & \text{in } \Omega_F, \\ p_k &= \overline{p}(t^{n+1}) & \text{on } \Gamma_F^1 \cup \Gamma_F^2, \\ \mathbf{u}_k \cdot \mathbf{n} &= 0 & \text{on } \Gamma_F^3, \\ p_k &= \phi_k & \text{on } \Sigma. \end{cases}$$

3. Update structure: find $\tilde{\eta}_k$ s.t.

$$\tilde{\eta}_k = \delta t \mathbf{u}_k \cdot \mathbf{n} + \eta^n \qquad \text{in } \Omega_S.$$

4. Relaxation step:

$$\eta_k = \omega \tilde{\eta}_k + (1-\omega)\eta_{k-1}.$$

5. Convergence test:

   - if $||\eta_k - \eta_{k-1}|| < tol$ then set $\eta^{n+1} = \eta_k$, $\mathbf{u}^{n+1} = \mathbf{u}_k$ and $p^{n+1} = p_k$
   - else set $k = k+1$ and go to step 1.

After elimination of $\mathbf{u}_k$ we have:

$$\mathcal{M_A}^{-1}\phi_k = \frac{\partial p_k}{\partial \mathbf{n}} = -\varrho_f \frac{(\mathbf{u}_k - \mathbf{u}^n)\cdot \mathbf{n}}{\delta t} = -\varrho_f \frac{\tilde{\eta}_k - 2\eta^n + \eta^{n-1}}{\delta t^2} \qquad \text{in } \Omega_S,$$

and

$$\begin{aligned} \frac{\varrho_f \mathcal{M_A}}{\delta t^2}\left(\frac{\eta_k}{\omega} - 2\eta^n + \eta^{n-1}\right) &= \frac{\varrho_f \mathcal{M_A}}{\delta t^2}\frac{(1-\omega)}{\omega}\eta_{k-1} \\ &\quad - \varrho_s h_s \frac{\eta_{k-1} - 2\eta^n + \eta^{n-1}}{\delta t^2} - a\eta_{k-1} + p_{ext}^{n+1}, \qquad k = 1, 2, \ldots \end{aligned}$$

or, equivalently, as the fixed-point method

$$\frac{\varrho_f \mathcal{M_A}}{\omega \delta t^2}\eta_k = \left[\frac{(1-\omega)}{\omega}\frac{\varrho_f \mathcal{M_A}}{\delta t^2} - \frac{\varrho_s h_s}{\delta t^2} - a\right]\eta_{k-1} + g(\eta^n, \eta^{n+1}, p_{ext}^{n+1}). \qquad (34)$$

Concerning the convergence of the fixed-point iteration (34), the following result holds.

Proposition 5 *The N-D iterative method converges to the solution to (28)-(30) if and only if, for all* $i = 1, 2, \ldots,$

$$\boxed{0 < \omega < \frac{2\varrho_f}{\varrho_f + (\varrho_s h_s + a\delta t^2)/\mu_i}} \tag{35}$$

Proof. The solution η^{n+1} to (28)-(30) is the fixed point of the iterative method (34) and a necessary and sufficient condition for the convergence of this latter is

$$\left| \frac{(1-\omega)\varrho_f \mu_i - \omega(\varrho_s h_s + a\delta t^2)}{\varrho_f \mu_i} \right| < 1.$$

A straightforward calculation leads to (35). □

Remark 6 *Notice that, at the continuous level, the infimum of the eigenvalues of* $\mathcal{M}_\mathcal{A}$ *is zero. At the discrete level,* $\mu^h_{min} = O(h)$*, where* h *denotes the space discretization parameter (see [18, 2]). Thus, the above result shows that the relaxation parameter* ω *for Neumann/Dirichlet iterations tends to zero with the space discretization parameter* h*. Therefore, such an algorithm seems not to be of practical use.*

7 Numerical results

In the following we present a series of numerical tests carried out on a code implementing the toy FSI problem and using the different time-marching schemes discussed in the previous sections. The aim of these tests is to provide a numerical validation of the above theoretical results. Before presenting the results, we need to introduce some further notation.

7.1 Space discretization

Here we consider the space discretization of the fluid problem (4) written in terms of the pressure only. The space discretization of problem (3) in velocity and pressure would lead to analogous results.

Let $\mathcal{T}_h$ be a regular triangulation of Ω_F made of quadrilaterals (denoted by K) and $\mathcal{J}_h$ be a partition of Ω_s made of intervals (denoted by J), conforming to the nodes of $\mathcal{T}_h$ lying on Σ. For ease of presentation, we can suppose $\mathcal{T}_h$ to be a regular Cartesian mesh such that its trace on Σ is made of equally spaced intervals. Moreover, we introduce the discrete spaces

$$\begin{aligned} Q_h &= \{q_h \in Q,\ q_h|_K \in \mathbb{Q}_1(K),\ \forall K \in \mathcal{T}_h\}, \\ V_h &= \{\xi_h \in V,\ \xi_h|_J \in \mathbb{P}_1(J),\ \forall J \in \mathcal{J}_h\}. \end{aligned} \tag{36}$$

Let us denote by $N_S = \dim(V_h)$ the number of structure nodes internal to Ω_s and by $N_F = \dim(Q_h)$ the number of fluid nodes internal to Ω_F or lying on Σ.

Denoting by A the fluid stiffness matrix, we have that the discrete fluid problem reads

$$AP = F, \tag{37}$$

where P is the vector of the nodal values of p_h. We can reorder the fluid nodes such that the internal ones come first, *i.e.* $I = \{1, 2, ..., N_F - N_S\}$ and $\Sigma = \{N_F - N_S + 1, N_F\}$. We indicate by P_I the vector of the first $N_F - N_S$ pressure values (pressure values at the interior of the fluid domain) and with P_Σ the remaining N_S boundary pressure values (pressure values on the fluid-structure interface). The above decomposition in internal and interface nodes reads

$$\begin{bmatrix} A_{II} & A_{I\Sigma} \\ A_{\Sigma I} & A_{\Sigma\Sigma} \end{bmatrix} \begin{bmatrix} P_I \\ P_\Sigma \end{bmatrix} = \begin{bmatrix} F_I \\ F_\Sigma \end{bmatrix}, \tag{38}$$

where F_I accounts for the external pressure at the entrance of the fluid domain and F_Σ is the discrete counterpart of the boundary term $-\varrho_f \displaystyle\int_\Sigma \frac{\partial^2 \eta}{\partial t^2} q \, ds$. Eliminating now the internal unknowns in favor of the interface ones and solving the resulting equation, yields the expression

$$P_\Sigma = M_A(F_\Sigma - A_{\Sigma I} A_{II}^{-1} F_I), \tag{39}$$

where $M_A = (A_{\Sigma\Sigma} - A_{\Sigma I} A_{II}^{-1} A_{I\Sigma})^{-1}$ is the discrete counterpart of the added-mass operator. Denoting by M_S and K_S the structure mass and stiffness matrices, respectively, the discrete structure problem reads

$$\varrho_s h_s M_S \ddot{D} + (bK_S + aM_S)D = M_S P_\Sigma, \tag{40}$$

where D is the vector of the nodal values of η_h. Using (39) and observing that $F_\Sigma = -\varrho_f M_S \ddot{D}$, we eventually end up with the following discrete interface problem of dimension N_S

$$(\varrho_s h_s M_S + \varrho_f M_S M_A M_S)\ddot{D} + (bK_S + aM_S)D = -M_S M_A (A_{\Sigma I} A_{II}^{-1} F_I). \tag{41}$$

We now apply to (41) the time discretization schemes discussed in the previous sections. The numerical tests are performed using geometrical and physical parameters pertinent to the case of blood flow in large arteries (see Tab. 4).

7.2 LF-EI time advancing scheme

Referring to the domain of Fig. 2, we set $R = 1\,\text{cm}$ and $L = 6\,\text{cm}$ and we take $h_s = 0.1\,\text{cm}$, $\varrho_f = 1\,\text{g/cm}^3$, $E = 0.75 \cdot 10^6\,\text{dynes/cm}^2$, $\nu = 0.5$. The fluid is initially at rest and an over-pressure of $2 \cdot 10^4 \text{dynes/cm}^2 (\simeq 15\text{mmHg})$ is imposed at the inlet for a duration of $0.005\,\text{s}$. A discretization step $h_x = 0.15\,\text{cm}$ in the x direction is considered. Evaluating the numerical value of μ_{max}, the limiting value of the structure density given by (26) turns out to be $(h_s \varrho_s)_{lim} \simeq 3.98\,\text{g/cm}^2$.

We observe the behavior of scheme (25) in the time interval $[0, T_{max} = 3\,\text{s}]$ for different values of the structure surface density $h_s \varrho_s$, ranging from below to

above the theoretical limiting value. The experimental results are collected in Tab. 1. In the greatest part of the situations, the instability occurs fairly before reaching T_{max}, and the smaller the structural density is (below the critical value) the sooner this phenomenon manifests. We also observe a slight dependence on the time step, and namely instability is reached earlier adopting a coarser time step. This effect is expected from the result of Proposition 3.

<table>
<tr><th>$h_s\varrho_s$ [g/cm^2]</th><th>$\delta t = 1e-3\,$s</th><th>$\delta t = 1e-4\,$s</th><th>$\delta t = 1e-5\,$s</th></tr>
<tr><td>4.5</td><td rowspan="2">stable</td><td rowspan="3">stable</td><td rowspan="3">stable</td></tr>
<tr><td>4.2</td></tr>
<tr><td>4.0</td><td rowspan="6">unstable</td></tr>
<tr><td>3.98</td><td rowspan="5">unstable</td><td rowspan="5">unstable</td></tr>
<tr><td>3.97</td></tr>
<tr><td>3.96</td></tr>
<tr><td>3.95</td></tr>
<tr><td>3.85</td></tr>
</table>

Table 1: Behavior of the LF-EI numerical scheme for different values of the structure density in the neighborhood of the value $(h_s\varrho_s)_{lim} = 3.98\text{g/cm}^2$.

The same behavior displayed in Tab. 1 is observed when h_x is varied (for example halved or doubled). Varying in turn L, while keeping R fixed, leads to analogous results, confirming that explicit numerical simulations of slender fluid-structure systems suffer from a more stringent lower limit for the structure surface density than bulky fluid-structure systems. Namely, in the case $L = 2\,$cm we find $(h_s\varrho_s)_{lim} \simeq 0.7\,\text{g/cm}^2$, while for $L = 10\,$cm we find $(h_s\varrho_s)_{lim} \simeq 10.46\,\text{g/cm}^2$.

Remark 7 *The numerical tests are pretty adherent to Proposition 3. In particular, they confirm the influence of geometry and density ratio on the stability of explicit scheme. Moreover, it must be observed that the value $\varrho_{s,lim}$ corresponding to $L = 6$ is considerably greater than the physiological arterial wall density (see also Tab. 4).*

Remark 8 *The results of Tab. 1 are very close to those in [16, Table 4.1, page 145], these latter corresponding to the full non-linear problem mentioned in Section 2, with the same choice of parameters. This is a strong confirmation that the reduced model investigated in this paper captures the main source of instability appearing in the non-linear FSI problem of interest in hemodynamics.*

7.3 Dirichlet-Neumann subiterations

We present the results of the numerical tests conducted using the iterative scheme presented in Section 6.1. Considering again the geometry and the discretization parameters of Sect. 7.2, we set $h_s\varrho_s = 3.0\,\text{g/cm}^2$, this value being well already in the domain of instability for the LF-EI scheme. From (33), we compute the upper limit value for the acceleration parameter $\omega_{lim} =$

$[0.922, 0.861, 0.8603]$ for the fixed point method, using $\delta t = [1e{-}3, 1e{-}4, 1e{-}5]$ s, respectively. We set to 2000 the maximum number of iterations allowed to satisfy the convergence test $||\eta_k - \eta_{k-1}|| < 1e-6$. The experimental results are collected in Tab. 2. The results are pretty in agreement with (33).

<table>
<tr><th>ω</th><th>$\delta t = 1e-3\,\mathrm{s}$</th><th>$\delta t = 1e-4\,\mathrm{s}$</th><th>$\delta t = 1e-5\,\mathrm{s}$</th></tr>
<tr><td>0.75</td><td rowspan="6">stable</td><td rowspan="3">stable</td><td rowspan="3">stable</td></tr>
<tr><td>0.8</td></tr>
<tr><td>0.85</td></tr>
<tr><td>0.86</td><td rowspan="6">unstable</td><td rowspan="6">unstable</td></tr>
<tr><td>0.87</td></tr>
<tr><td>0.88</td></tr>
<tr><td>0.89</td></tr>
<tr><td>0.91</td></tr>
<tr><td>0.922</td><td rowspan="3">unstable</td></tr>
<tr><td>0.93</td></tr>
<tr><td>0.91</td></tr>
</table>

Table 2: Behavior of the iterative scheme (32) for different values of the acceleration parameter ω in the neighborhood of the limit $\omega_{lim} = [0.922, 0.861, 0.8603]$.

An analogous behavior is observed for different values of the discretization parameter h_x and for different values of ϱ_s.

7.4 Neumann/Dirichlet subiterations

Finally, we present the results of the numerical tests conducted using the procedure (34). Again, we consider the same domain and the same physical parameters as before. Setting $h_s \varrho_s = 3.0\,\mathrm{g/cm^2}$ and using space steps $h_x = [L/20, L/40, L/60]$ from (35) we find that $\omega_{lim} = [0.0459, 0.0221, 0.0135]$, respectively. In Tab. 3 we show the results obtained with a time step $\delta t = 10^{-4}$s and $||\eta_k - \eta_{k-1}|| < 1e-6$ (max number of iterations is 2000). In particular, we find confirmation of the fact that in this case $\omega = \omega(h)$, this implying that in the limit $h \to 0$, ω must also tend to zero! We also observe that, in order to observe the onset of instability as prescribed by the theoretical results, in some cases it should be necessary to integrate for a time interval longer than $T_{max} = 3\,\mathrm{s}$. For coherence with the previous results, we limit our analysis to this latter value.

<table>
<tr><th>ω</th><th>h_x=L/20</th><th>h_x=L/40</th><th>h_x=L/60</th></tr>
<tr><td>0.058</td><td rowspan="4">unstable</td><td rowspan="8">unstable</td><td rowspan="14">unstable</td></tr>
<tr><td>0.057</td></tr>
<tr><td>0.056</td></tr>
<tr><td>0.055</td></tr>
<tr><td>0.05</td><td rowspan="13">stable</td></tr>
<tr><td>0.0459</td></tr>
<tr><td>0.03</td></tr>
<tr><td>0.025</td></tr>
<tr><td>0.02445</td></tr>
<tr><td>0.023</td><td rowspan="11">stable</td></tr>
<tr><td>0.0221</td></tr>
<tr><td>0.0215</td></tr>
<tr><td>0.02</td></tr>
<tr><td>0.014</td></tr>
<tr><td>0.0139</td></tr>
<tr><td>0.0137</td></tr>
<tr><td>0.0135</td><td rowspan="3">stable</td></tr>
<tr><td>0.0130</td></tr>
<tr><td>0.0125</td></tr>
</table>

Table 3: Behavior of the Neumann-Dirichlet scheme as the spatial discretization parameter tends to zero.

8 Characterization of the numerical properties of partitioned schemes through dimensional analysis

The analysis carried out in the preceding sections shows the dependence of the numerical stability of the solution of the added-mass problem on the values of the physical parameters. To highlight this fact, another possible way to proceed is proposed in [15, 10], where scaling arguments are used to provide indications about the influence of the physical parameters. This analysis applies to the linear case. In the present section we will pursue a similar approach. This will allow, on the one hand, to put in the frame of [15, 10] the results of the present discussion, and on the other hand, to devise a more general point of view with respect to the analysis of Sect. 6 - even if more qualitative - in presence for example of a non-negligible second order term $\partial^2\eta/\partial x^2$. We observe that this latter is the situation that actually corresponds to the one studied in [15, 10], where, differently from the present analysis, inertial terms were neglected.

We introduce the characteristic length and velocity scales L_m, U_m and we

define the following non-dimensional quantities

$$(\widetilde{x},\widetilde{y},\widetilde{z})^T = \frac{(x,y,z)^T}{L_m}, \quad \widetilde{u} = \frac{u}{U_m}, \quad \widetilde{\eta} = \frac{\eta}{L_m}$$

and

$$\delta t_* = \frac{U_m}{L_m}\delta t, \qquad \widetilde{p} = \frac{p}{\varrho_F U_m^2}.$$

In the case of blood flow in large arteries in a human body, pertinent characteristic parameters are reported in Tab. 4.

Parameter	Value
Reference length: L_m	6 cm
Reference radius: R	0.5 cm
Mean velocity: U_m	10 cm/s
Blood density: ϱ_f	1 g/cm^3
Wall density: $h_s\varrho_s$	1.1 g/cm^2
Wall thickness: h_s	0.1 cm
Shear modulus: $k_T G$	2.5×10^5 dynes/cm^2
Young modulus: E	0.75×10^6 dynes/cm^2
Poisson coefficient: ν	0.5

Table 4: Physical parameter values for blood flow in large arteries in human body.

From the time discretized form of equation (18)

$$p_\Sigma = -\varrho_f \mathcal{M}_A \frac{\eta}{\delta t^2} + g, \tag{42}$$

where g groups the forcing term p_{ext} and the terms coming form the previous time steps, we have that the adimensional added-mass operator reads

$$\widetilde{\mathcal{M}}_A = \frac{\mathcal{M}_A}{L_m} \qquad \text{and} \qquad \mathcal{M}_A \frac{\eta}{\delta t^2} = \frac{U_m^2}{\delta t_*^2}\widetilde{\mathcal{M}}_A \widetilde{\eta}. \tag{43}$$

The time discretized structure equation reads

$$S_S \eta = \left(\frac{\varrho_s h_s}{\delta t^2}\mathcal{I} + \mathcal{L}\right)\eta = p_\Sigma, \tag{44}$$

where we have introduced the symmetric and positive operator S_S, for which we propose the following scaling

$$\widetilde{S}_S\widetilde{\eta} = \frac{\delta t_*^2 L_m}{\varrho_s h_s U_m^2} S_S \eta = \widetilde{\eta} - \frac{\delta t_*^2 k_T G}{\varrho_s U_m^2}\frac{\partial^2 \widetilde{\eta}}{\partial \widetilde{z}^2} + \frac{\delta t_*^2 E L_m^2}{R^2(1-\nu^2)\varrho_s U_m^2}\widetilde{\eta}, \tag{45}$$

that yields

$$S_S \eta = \frac{\varrho_s h_s U_m^2}{\delta t_*^2 L_m}\widetilde{S}_S\widetilde{\eta}. \tag{46}$$

Remark 9 *We observe that, with the present model, the ratio* $k_1 = \dfrac{\delta t_*^2 k_T G}{\varrho_s U_m^2} = \dfrac{\delta t^2 k_T G}{\varrho_s L_m^2}$ *measures the relative influence of the elastic shear terms and of the inertial terms, while the ratio* $k_2 = \dfrac{\delta t_*^2 E L_m^2}{R^2(1-\nu^2)\varrho_s U_m^2} = \dfrac{\delta t^2 E}{R^2(1-\nu^2)\varrho_s}$ *measures the relative influence of the elastic stiffness terms and of the inertial terms.*

If we now gather (43) - (46), we obtain the adimensional form of the FSI problem

$$\widetilde{S}\widetilde{\eta} = \left(\widetilde{S}_S + \frac{\varrho_f L_m}{\varrho_s h_s}\widetilde{\mathcal{M}}_A\right)\widetilde{\eta} = \widetilde{\mathcal{F}}. \tag{47}$$

where $\widetilde{\mathcal{F}}$ accounts for known terms. Problem (47) is approximated in finite dimension by

$$\widetilde{S}^h\widetilde{\eta}^h = (\widetilde{S}_S^h + \frac{\varrho_f L_m}{\varrho_s h_s}\widetilde{\mathcal{M}}_A^h)\widetilde{\eta}^h = \widetilde{\mathcal{F}}^h, \tag{48}$$

where the operator $\widetilde{S}^h$ is symmetric and positive definite. The iterative fixed point method (32), introduce in Sect. 6.1, reads in this context (for simplicity, we omit the h superscript):
given $\widetilde{\eta}^k, k \geq 0$, compute

$$\begin{cases} \delta\widetilde{\eta} = \widetilde{S}_S^{-1}\widetilde{\mathcal{F}} - \dfrac{\varrho_f L_m}{\varrho_s h_s}\widetilde{S}_S^{-1}\widetilde{\mathcal{M}}_A\widetilde{\eta}^k, \\ \widetilde{\eta}^{k+1} = (1-\omega)\widetilde{\eta}^k + \omega\delta\widetilde{\eta}, \end{cases} \tag{49}$$

that is

$$\widetilde{\eta}^{k+1} = \omega\widetilde{S}_S^{-1}\widetilde{\mathcal{F}} + [I_d - \omega P]\widetilde{\eta}^k, \tag{50}$$

where we have set

$$P = \widetilde{S}_S^{-1}\widetilde{S} = \big[I_d + \frac{\varrho_f L_m}{\varrho_s h_s}\widetilde{S}_S^{-1}\widetilde{\mathcal{M}}_A\big].$$

The choice $\omega = 1$ means adopting a non-relaxed fixed-point algorithm to solve the coupled problem.

As, in general, the matrix P is not symmetric, it is convenient to perform the substitution $\widehat{\eta} = \widetilde{S}_S^{1/2}\widetilde{\eta}$; this procedure leads to the form

$$\widehat{\eta}^{k+1} = \omega\widetilde{S}_S^{-1/2}\widetilde{\mathcal{F}} + \left(I_d - \omega\left[I_d + \frac{\varrho_f L_m}{\varrho_s h_s}\widetilde{S}_S^{-1/2}\widetilde{\mathcal{M}}_A\widetilde{S}_S^{-1/2}\right]\right)\widehat{\eta}^k, \tag{51}$$

that corresponds to applying the gradient algorithm with fixed acceleration parameter to the symmetric positive definite operator

$$\widehat{P} = \big[I_d + \frac{\varrho_f L_m}{\varrho_s h_s}\widetilde{S}_S^{-1/2}\widetilde{\mathcal{M}}_A\widetilde{S}_S^{-1/2}\big].$$

Denoting by $(\mathcal{A})_{max}$ the extremal eigenvalues of the operator $\mathcal{A}$, a necessary and sufficient condition (see [18], p. 38) for the convergence of the fixed point method with constant acceleration parameter ω is the following

Proposition 6 *The fixed point algorithm* (49) *converges linearly toward the solution of the linearized implicit coupled problem at time* t^{n+1} *if and only if*

$$0 < \omega < \frac{2\varrho_s h_s/\varrho_f L_m}{\left(\frac{\varrho_s h_s}{\varrho_f L_m} Id + \widetilde{S}_S^{-1/2} \widetilde{\mathcal{M}}_A \widetilde{S}_S^{-1/2}\right)_{max}} \tag{52}$$

Remark 10 *A fixed point algorithm applied to the solution of the coupled system requires to use a smaller value of the relaxation parameter as the density of the fluid approaches the density of the structure, this limitation being not dependent on the choice of the time step. This qualitative result is in agreement with the analysis carried out in Sect. 6.1.*

The above procedure allows as well to see what happens if we were instead in the case of dominant stiffness terms in the structure, that is if $k_2 >> 1$. To do this, we should change the scaling and in particular we need to introduce a characteristic stiffness $E_m = E$. We perform accordingly the scaling of the structure operator, yielding

$$S_S \eta = \frac{E_m L_m^2}{R^2(1-\nu^2)} \widetilde{S}_S \widetilde{\eta} \tag{53}$$

and thus

$$\widetilde{S}\widetilde{\eta} = \left(\widetilde{S}_S + \frac{\varrho_f U_m^2 R^2 (1-\nu^2)}{\delta t_*^2 E_m L_m^2} \widetilde{\mathcal{M}}_A\right) \widetilde{\eta} = \widetilde{\mathcal{F}}. \tag{54}$$

Proceeding analogously as in the case of dominating inertial terms, we may write the following relaxed fixed point method:
given $\widetilde{\eta}^k, k \geq 0$, compute

$$\begin{cases} \delta\widetilde{\eta} = \widetilde{S}_S^{-1}\widetilde{\mathcal{F}} - \dfrac{\varrho_f U_m^2 R^2(1-\nu^2)}{\delta t_*^2 E_m L_m^2} \widetilde{S}_S^{-1} \widetilde{\mathcal{M}}_A \widetilde{\eta}^k, \\ \widetilde{\eta}^{k+1} = (1-\omega)\widetilde{\eta}^k + \omega \delta\widetilde{\eta}, \end{cases} \tag{55}$$

that is

$$\widetilde{\eta}^{k+1} = \omega \widetilde{S}_S^{-1} \widetilde{\mathcal{F}} + [I_d - \omega P]\widetilde{\eta}^k, \tag{56}$$

where we have set

$$P = \widetilde{S}_S^{-1}\widetilde{S} = \left[I_d + \frac{\varrho_f U_m^2 R^2(1-\nu^2)}{\delta t_*^2 E_m L_m^2} \widetilde{S}_S^{-1} \widetilde{\mathcal{M}}_A\right].$$

Operating again the change of variables $\widehat{\eta} = \widetilde{S}_S^{1/2}\widetilde{\eta}$, such that the corresponding operator $\widehat{\eta}$ is symmetric and positive definite, we have that the following proposition holds.

Proposition 7 *The fixed point algorithm* (55) *converges linearly toward the solution of the linearized implicit coupled problem at time* t^{n+1} *if and only if*

$$0 < \omega < \frac{2\dfrac{\delta t_*^2 E_m L_m}{\varrho_f U_m^2 R^2(1-\nu^2)}}{\left(\dfrac{\delta t_*^2 E_m L_m}{\varrho_f U_m^2 R^2(1-\nu^2)} Id + \widetilde{S}_S^{-1/2} \widetilde{\mathcal{M}}_A \widetilde{S}_S^{-1/2}\right)_{max}}. \tag{57}$$

Remark 11 *This result is analogous to what found in [15, 10]. We observe in particular that in this case a fixed point algorithm requires a smaller relaxation parameter for a soft structure or for a small time step ($E_m \delta t_*^2$ small) or again as the fluid density increases.*

Acknowledgments:
This work has been partially supported by the *Research Training Network* "Mathematical Modelling of the Cardiovascular System" (HaeMOdel), contract HPRN-CT-2002-00270 of the European Community.

References

[1] P.E. Bjorstad and O.B. Widlund. Iterative methods for the solution of elliptic problems on regions partitioned in subdomains. *SIAM J. Numer. Anal.*, 31(23):1097–1120, 1986.

[2] S. Brenner. The condition number of the Schur complement in domain decomposition. *Numerische Mathematik*, 83(2):187–203, 1999.

[3] H. Brezis. *Analyse fonctionnelle, Théorie et applications*. Masson, 1983.

[4] C. Farhat, M. Lesoinne, and P. Le Tallec. Load and motion transfer algorithms for fluid/structure interaction problems with non-matching discrete interfaces: Momentum and energy conservation, optimal discretization and application to aeroelasticity. *Comput. Methods Appl. Mech. Engrg.*, 157:95–114, 1998.

[5] C. Farhat, K. van der Zee, and Ph. Geuzaine. Provably second-order time-accurate loosely-coupled solution algorithms for transient nonlinear aeroelasticity. in preparation.

[6] L. Formaggia, J.-F. Gerbeau, F. Nobile, and A. Quarteroni. On the coupling of 3D and 1D Navier-Stokes equations for flow problems in compliant vessels. *Comp. Meth. Appl. Mech. Engrg.*, 191(6-7):561–582, 2001.

[7] J.F. Gerbeau and M. Vidrascu. A Quasi-Newton algorithm based on a reduced model for fluid-structure interactions problems in blood flows. *Math. Model. Num. Anal.*, 37(4):631–648, 2003.

[8] M. H. Holmes. A spectral problem in hydroelasticity. *J. Differential Equations*, 32(3):388–397, 1979.

[9] P. Le Tallec. *Introduction à la dynamique des structures*. Ellipses, 2000.

[10] P. Le Tallec and J. Mouro. Fluid structure interaction with large structural displacements. *Comput. Meth. Appl. Mech. Engrg.*, 190:3039–3067, 2001.

[11] H.G. Matthies and J. Steindorf. Partitioned but strongly coupled iteration schemes for nonlinear fluid-structure interaction. *Computers and Structures*, 80(27–30):1991–1999, 2002.

[12] D. P. Mok, W. A. Wall, and E. Ramm. Accelerated iterative substructuring schemes for instationary fluid-structure interaction. In K.J. Bathe, editor, *Computational Fluid and Solid Mechanics*, pages 1325–1328. Elsevier, 2001.

[13] H. Morand and R. Ohayon. *Interactions fluides-structures*, volume 23 of *Recherches en Mathématiques Appliquées*. Masson, Paris, 1992.

[14] H. Morand and R. Ohayon. *Fluid-Structure Interaction: Applied Numerical Methods*. John Wiley & Sons, 1995.

[15] J. Mouro. *Interactions fluide structure en grands déplacements. Résolution numérique et application aux composants hydrauliques automobiles*. PhD thesis, Ecole Polytechnique, France, 1996.

[16] F. Nobile. *Numerical approximation of fluid-structure interaction problems with application to haemodynamics*. PhD thesis, EPFL, Switzerland, 2001.

[17] S. Piperno, C. Farhat, and B. Larrouturou. Partitioned procedures for the transient solution of coupled aeroelastic problems. Part I: Model problem, theory and two-dimensional application. *Comp. Meth. Appl. Mech. Engrg.*, 124:79–112, 1995.

[18] A. Quarteroni and A. Valli. *Domain decomposition methods for partial differential equations*. Numerical Mathematics and Scientific Computation. The Clarendon Press Oxford University Press, 1999. Oxford Science Publications.

[19] S. Rugonyi and K.J. Bathe. On finite element analysis of fluid flows coupled with structural interaction. *CMES - Comp. Modeling Eng. Sci.*, 2(2):195–212, 2001.

[20] K. Stein, R. Benney, V. Kalro, T.E. Tezduyar, J. Leonard, and M. Accorsi. Parachute fluid-structure interactions: 3-D computation. *Comput. Methods Appl. Mech. Engrg.*, 190(3–4):373–386, 2000.

[21] H. Zhang, X. Zhang, S. Ji, Y. Guo, G. Ledezma, N. Elabbasi, and H. deCougny. Recent development of fluid-structure interaction capabilities in the adina system. *Computers and Structures*, 81(8–11):1071–1085, 2003.